

# Electronic structure of optimally doped pnictide $\text{Ba}_{0.6}\text{K}_{0.4}\text{Fe}_2\text{As}_2$ : a comprehensive ARPES investigation

H. Ding,<sup>1</sup> K. Nakayama,<sup>2</sup> P. Richard,<sup>3</sup> S. Souma,<sup>3</sup> T. Sato,<sup>2,4</sup> T. Takahashi,<sup>2,3</sup> M. Neupane,<sup>5</sup> Y.-M. Xu,<sup>5</sup> Z.-H. Pan,<sup>5</sup> A.V. Federov,<sup>6</sup> Z. Wang,<sup>5</sup> X. Dai,<sup>1</sup> Z. Fang,<sup>1</sup> G.F. Chen,<sup>1</sup> J.L. Luo,<sup>1</sup> and N.L. Wang<sup>1</sup>

(1) *Beijing National Laboratory for Condensed Matter Physics, and Institute of Physics, Chinese Academy of Sciences, Beijing 100190, China*

(2) *Department of Physics, Tohoku University, Sendai 980-8578, Japan*

(3) *WPI Research Center, Advanced Institute for Materials Research, Tohoku University, Sendai 980-8577, Japan*

(4) *TRIP, Japan Science and Technology Agency (JST), Kawaguchi 332-0012, Japan*

(5) *Department of Physics, Boston College, Chestnut Hill, MA 02467, USA*

(6) *Advanced Light Source, Lawrence Berkeley National Laboratory, Berkeley, CA 94720*

(Dated: July 26, 2021)

## Abstract

We have conducted a comprehensive angle-resolved photoemission study on the normal state electronic structure of the Fe-based superconductor  $\text{Ba}_{0.6}\text{K}_{0.4}\text{Fe}_2\text{As}_2$ . We have identified four dispersive bands which cross the Fermi level and form two hole-like Fermi surfaces around  $\Gamma$  and two electron-like Fermi surfaces around M. There are two nearly nested Fermi surface pockets connected by an antiferromagnetic  $(\pi, \pi)$  wavevector. The observed Fermi surfaces show small  $k_z$  dispersion and a total volume consistent with Luttinger theorem. Compared to band structure calculations, the overall bandwidth is reduced by a factor of 2. However, many low energy dispersions display stronger mass renormalization by a factor of  $\sim 4$ , indicating possible orbital (energy) dependent correlation effects. Using an effective tight banding model, we fitted the band structure and the Fermi surfaces to obtain band parameters reliable for theoretical modeling and calculations of the important physical quantities, such as the specific heat coefficient.

PACS numbers: 74.25.Jb, 74.70.-b, 79.60.-i

The recent discovery of superconductivity in iron pnictides has opened a new route to high temperature superconductivity beyond the cuprates [1]. It is now widely believed that the multiband nature of this material is important, pertaining to the superconducting instability in the doped compound and the antiferromagnetic (AF) spin density wave (SDW) instability [2] in the parent compound. The knowledge of the electronic band structure and Fermi surface (FS) topology is critical to understanding the underlying physics. Most first-principle band theory calculations, such as local density approximation (LDA) [3, 4, 5], have predicted that five bands of the Fe  $3d t_{2g}$  complex cross the Fermi level ( $E_F$ ), and form three hole-like FSs centered at the zone center ( $\Gamma$ ) and two electron-like FSs centered at the zone corner (M). However, there remain inconsistencies in the predicted band structure [6]. More seriously, the optimal As position calculated in LDA is quite different (more than 10%) from the experimental value [6]. On the experimental side, angle-resolved photoemission spectroscopy (ARPES) studies [7, 8, 9, 10, 11, 12, 13, 14] have observed several dispersive bands and FSs, showing some consistencies with LDA calculations. However, some major discrepancies exist and a quantitative comparison is lacking. In particular, there is no consensus regarding the band structure and FS near the M point. In order to resolve these controversies and thus obtain comprehensive knowledge of the electronic structure of the iron pnictides, we have carried out a systemic ARPES study on an optimally doped superconductor  $\text{Ba}_{0.6}\text{K}_{0.4}\text{Fe}_2\text{As}_2$ .

The high-quality single crystals of  $\text{Ba}_{0.6}\text{K}_{0.4}\text{Fe}_2\text{As}_2$  ( $T_c = 37$  K) used in this study were grown by the flux method [15]. These are the same samples used to determine the FS-dependent nodeless superconducting gaps that close at the bulk  $T_c$  [7]. Low-energy electron diffraction on a mirror-like cleaved surface shows a sharp  $1 \times 1$  pattern without any detectable reconstruction down to 20 K. All of these indicate that the cleaved surface on this material retains a bulk-representative electronic structure. High-resolution (4 - 20 meV) ARPES measurements were performed in the photoemission laboratory of Tohoku University using a microwave-driven Helium source ( $h\nu = 21.218$  eV), and several synchrotron beamlines in the Synchrotron Radiation Center and the Advanced Light Source in the US, and the Photon Factory in Japan, using various photon energies ranging from 20 eV to 100 eV to selectively enhance different band features of this multiband system. Samples were cleaved *in situ* at low temperature (10 - 40 K) and measured at 7 - 150 K in a working vacuum better than  $1 \times 10^{-10}$  Torr.

We start with a wide energy spectrum (Fig. 1a) that includes shallow core levels and the valence band, which can yield valuable information on the valence and chemical environment of the constituent elements. The strong double peaks at the binding energies of 40.4 and 41.1 eV are from As  $3d_{5/2}$  and  $3d_{3/2}$ , the same as the  $3d$  core levels of As in bulk GaAs (40.4 and 41.1 eV) [16]. However, unlike GaAs (110) that has a surface component in the As  $3d$  core levels,  $\text{Ba}_{0.6}\text{K}_{0.4}\text{Fe}_2\text{As}_2$  shows no clear evidence for a second component of As  $3d$ , suggesting no major surface modification involving the As atoms. We have also identified several other core levels, such as Fe  $3p$  (52.4, 53.0 eV), K  $3s$  (33.0 eV) and  $3p$  (17.8 eV), Ba  $5s$  (29.7 eV) and  $5p$  (14.2, 16.2 eV), and As  $4s$  (16.9 eV). In addition, there is a weak but well-defined peak at 12 eV, as shown in the inset of Fig. 1a, which has also been observed in our measurements of the parent compounds  $\text{BaFe}_2\text{As}_2$  and  $\text{SrFe}_2\text{As}_2$ . A peak at a similar binding energy has been observed in divalent iron compounds, such as FeO [17], which has been attributed to a satellite state with the Fe  $3d^5$  configuration. A valence satellite state, such as the well-known 11 eV Cu  $3d^8$  satellite observed in many cuprate superconductors, has been attributed to strong correlation effects. The observation of the 12 eV satellite peak suggests the importance of the local electronic correlations at the Fe sites in the pnictides.

The valence band shows a strong photon energy dependence. Comparing energy distribution curves (EDCs) measured at 100 eV (enhancing the intensity of Fe  $3d$ ) and the ones measured at 21.2 eV (enhancing the intensity of As  $4p$ ), one can conclude that the strong peak within 1 eV from  $E_F$  is mostly from Fe  $3d$  orbitals, and the states behind it are mostly from As  $4p$ , consistent with the LDA calculations [18]. The valence band intensity undergoes a strong variation, or a resonance, when the photon energy is scanned through the Fe  $3p$  absorption edge ( $\sim 56$  eV), as seen in Fig. 1b. Following a common practice in photoemission [17], we plot in Fig. 1b the difference between EDCs measured at 56 eV (at resonance) and 52 eV (below resonance), which corresponds mostly to Fe  $3d$  states since the intensity of other orbitals is not expected to change drastically over this narrow photon energy window [19]. The difference curve shows a sharp peak at  $E_F$  which corresponds to the coherent Fe  $3d$  orbitals, and a broad peak centered at  $\sim 7$  eV which can be regarded as the incoherent part of Fe  $3d$  states. The assignment of coherent and incoherent components is also supported by the observation in Fig. 1c of the “anti-resonance” profile of the coherent part and the Fano-like resonance profile for the incoherent part at 7 eV and 12 eV (satellite peak) due to super-Coster-Kronig Fe  $3p$ - $3d$  Auger transition, similar to what has been observation in FeO

[17]. The large incoherent component of Fe 3*d* at high binding energy is an indication of relatively strong correlation effects in this material. The correlation effects are also reflected from the observation that the coherent part of Fe 3*d* is compressed to 1 eV below  $E_F$  (see Fig. 1c) from the 2 eV range predicted by LDA. We note that this narrowing effect has been predicted by a dynamic mean field theory (DMFT) calculation which assumes large correlation effects [20].

Within the coherent Fe 3*d* region, we observe several dispersive bands, as shown in Fig. 2 which displays band dispersions along several high symmetry directions ( $\Gamma$ -M,  $\Gamma$ -X, and M-X) determined using the EDCs (Figs. 2a, b),  $E$  vs  $k$  intensity plots (Figs. 2c, d), and second derivative plot (Fig. 2e), and the extracted EDC peak positions (Fig. 2f). We also plot the band dispersion calculated from our LDA [5] at this doping level. The LDA bands, when normalized (divided) by a factor of 2, agree well with the overall measured Fe 3*d* bands, especially for the high energy (0.2 - 0.6 eV) branches, as indicated in Fig. 2f. This band narrowing factor of 2, similar to an earlier ARPES observation in a pnictide (LaFeOP) [12], indicates the importance of correlation effects as seen in the multiorbital cobaltates [21]. However, we observe additional mass renormalization for the lower energy branches (below 0.2 eV) as shown in Fig. 2f and discussed in more details below, suggesting a possible stronger and/or orbital (energy) dependent correlation effect.

In order to accurately determine the low-energy band structure and the FS, we have performed high-resolution ARPES measurements in the vicinity of  $E_F$ , as shown in Fig. 3. Fig. 3a is an  $E$  vs  $k$  intensity plot near the  $\Gamma$  point, which clearly shows two dispersing bands ( $\alpha$  and  $\beta$ ) forming two hole-like FS pockets around  $\Gamma$ . This spectrum is measured in the superconducting state where the quasiparticle (QP) peak width is much narrower and the separation of the  $\alpha$  and  $\beta$  bands is more visible. However, we did not observe a third band predicted by LDA calculations, suggesting that it may be degenerated with either the  $\alpha$  or  $\beta$  band. The narrow QP peak and high resolution put an upper limit of 10 meV to the band splitting between the two overlapping bands in the vicinity of  $E_F$ . We have observed the top of the  $\alpha$  band at the  $\Gamma$  point by measuring it at high temperature ( $T = 150$  K) and dividing the spectrum by the Fermi function. As shown in Fig. 3b, this procedure unmasks the spectrum within a few  $k_B T$  above  $E_F$ , showing a clear parabola with the band top situated at  $\sim 20$  meV above  $E_F$ . This band top is much lower than the value of  $\sim 120$  meV predicted by LDA calculations.

The band structure near M has been controversial. While LDA predicted two electron-like Fermi surfaces around M, earlier ARPES studies claimed to have observed a hole-like dispersion [11, 13]. Using high-resolution ARPES, in Figs. 3c and d, we identify two electron-like bands (labeled as  $\gamma$  and  $\delta$  bands) with the bottoms at  $\sim 15$  and  $60$  meV, respectively. The energy difference between the observed  $\alpha$  band top and  $\gamma$  band bottom is about  $35$  meV, much smaller than the value of  $\sim 200$  meV predicted by LDA [18]. In addition, we observe in Fig. 3c a third band dispersing toward  $E_F$  when moving from  $\Gamma$  to M, intersecting with the  $\delta$  band in the vicinity of  $E_F$ . The anti-crossing of the two bands, or a Dirac point, near M has been predicted by LDA, as can be seen in the Fig. 4e. However, it occurs at a much higher binding energy ( $\sim 120$  meV). This uplifting of the Dirac point also creates a “bright” spot with a strong intensity at  $E_F$  observed in previous ARPES measurements [7, 11, 13].

We summarize our measurements of the FSs and the band structure in Fig. 4. By measuring many cuts in the Brillouin zone (BZ), we have obtained the FSs of  $\text{Ba}_{0.6}\text{K}_{0.4}\text{Fe}_2\text{As}_2$ . Fig. 4a displays the ARPES intensity integrated within a narrow energy window at  $E_F$  ( $\pm 10$  meV), where the high intensity contours are expected to follow the FS contours. We also extracted the  $k_F$  points from the dispersive bands indicated by the dots in Fig. 4a and obtained from both the momentum distribution curves (MDCs) and the EDCs. These extracted  $k_F$  points, in agreement with the high-intensity contours, clearly show four FS sheets. The hole-like  $\alpha$  and  $\beta$  FSs centered at  $\Gamma$  enclose areas of  $4\%$  and  $18\%$  of the BZ area, while the electron-like  $\gamma$  and  $\delta$  FSs centered at M have areas of  $2\%$  and  $4\%$ , respectively. According to Luttinger theorem on two-dimensional (2D) FS sheets, the observed four FS sheets correspond to  $16\%$  hole/Fe. The  $40\%$  K content in this optimally doped superconductor corresponds to  $20\%$  hole/Fe, suggesting that the fifth FS sheet predicted by LDA would be degenerated with the  $\alpha$  FS, yielding a total Luttinger area of  $20\%$  hole/Fe.

The above analysis of Luttinger area is under the assumption of 2D FS. However, LDA calculations predict significant  $k_z$  dispersions [18]. To check this, we have measured the  $\alpha$  and  $\beta$  FSs using different photon energies, or equivalently, at different values of  $k_z$ . The results are shown in Fig. 4b where the extracted FS areas are plotted as functions of  $k_z$ , which are estimated by using the free-electron final state approximation with a  $10$  eV inner potential. From Fig. 4b we do not observe a strong periodic variation of the FS area as  $k_z$  is changed, in contrast to the LDA prediction of strong  $k_z$ -dependent FS sheets. The

quasi-2D FSs are thought to be at odds with the isotropic upper critical field ( $H_{c2}$ ) derived from a high-field measurement [22]. However, a recent sensitive magnetic torque experiment on high-quality single crystals has observed a larger anisotropy between the  $a$ - $b$  plane and the  $c$ -axis [23].

We plot our measurements of band dispersion along the two high-symmetry lines ( $\Gamma$ -M and  $\Gamma$ -X) in Fig. 4e. As a comparison, we also plot the LDA bands renormalized by a factor of 2. While there is a fairly good agreement on the Fermi crossing ( $k_F$ ) between the ARPES measurements and LDA calculations, the Fermi velocity ( $v_F$ ) is further renormalized as compared to the renormalized LDA bands. In the table of Fig. 4c, we list the values of  $v_F$  along  $\Gamma$ -M obtained from ARPES measurement and LDA calculations. Most low energy bands have a mass renormalization greater than 4, significantly larger than the overall band renormalization obtained at high binding energy. This additional renormalization at low energy, which has also been observed in both cuprates and cobaltates [21, 24], can be attributed to an enhanced self-energy effect near  $E_F$ . Possible causes of the enhanced self-energy near  $E_F$  include electronic correlation effects, low-energy modes or fluctuations, and band hybridization. Independent of its microscopic origin, the small renormalized Fermi velocity has an important consequence on the superconducting coherence length, which can be estimated from the BCS relation  $\xi = \frac{\hbar v_F}{\pi \Delta}$ . From the obtained values of  $v_F$  and the measured superconducting gaps [7], we estimate that the coherence length in this superconductor is about 9 - 14 Å, which agrees well with the value ( $\sim 12$  Å) obtained from the  $c$ -axis upper critical field [25]. It is remarkable that the superconducting coherence length in this pnictide is much smaller than conventional BCS superconductors, and surprisingly close to that found in the cuprate superconductors.

Basic band parameters of this material constitute important starting point for microscopic and phenomenological theories of its unusual superconductivity and other instabilities. After determining the band structure and the FSs, we can now extract the dispersion parameters. Here we adapt a simple tight-binding-like band structure proposed previously [26]:  $E^{\alpha,\beta}(k_x, k_y) = E_0^{\alpha,\beta} + t_1^{\alpha,\beta}(\cos k_x + \cos k_y) + t_2^{\alpha,\beta} \cos k_x \cos k_y$ , and  $E^{\gamma,\delta}(k_x, k_y) = E_0^{\gamma,\delta} + t_1^{\gamma,\delta}(\cos k_x + \cos k_y) + t_2^{\gamma,\delta} \cos(k_x/2) \cos(k_y/2)$ . Under mild constraints for the unoccupied bands which are not accessible by ARPES, we obtain the band parameters for the four observed bands which are listed in the table in Fig. 4e. As shown in Figs. 4d and e, the FS contours and the band structure generated from these parameters

match remarkably well with the observed FSs and band dispersions. Note that the fitted FSs for the electron-like bands in the vicinity of M are two ellipses without including the effects of band hybridization between them. The latter splits the two bands and give rise to the observed outer ( $\delta$ ) and inner ( $\gamma$ ) FSs. As seen clearly in Fig. 4d, the  $\alpha$  FS, when shifted by the  $(\pi, \pi)$  wavevector, overlaps well with the  $\delta$  FS, strongly suggesting a good FS nesting with the same nesting wavevector  $(\pi, \pi)$  as the AF wavevector observed in the parent compound [2]. Combined with the observation of nearly identical superconducting gaps on the  $\alpha$ ,  $\delta$ , and  $\gamma$  FSs [7, 33] in the same material, this result reinforces the notion that the interband scattering among the nested Fermi surfaces plays a dominant role in the pairing interaction [27, 28, 29, 30].

One application for these band parameters is the estimate of the effective masses of the low energy bands, whose average values along the FSs are obtained:  $m_\alpha^* = 4.8$ ,  $m_\beta^* = 9.0$ ,  $m_\gamma^* = 1.3$ ,  $m_\delta^* = 1.3$ , in units of free electron mass. From these effective masses, we deduce the Sommerfeld parameter of the specific heat by using  $\gamma = \pi N_A K_B^2 a^2 m^* / 3\hbar^2$  (where  $a = 3.92$  Å is the lattice parameter and  $N_A$  is Avogadro's number), which are 7.2, 13.6, 2, 2 in units of mJ/K<sup>2</sup>mol for the  $\alpha$ ,  $\beta$ ,  $\gamma$ ,  $\delta$  bands, respectively. The total value of the  $\gamma$  coefficient, assuming doubly degenerated  $\alpha$  bands, is  $\sim 32$  mJ/K<sup>2</sup>mol, which is much larger than the value ( $\sim 9$  mJ/K<sup>2</sup>mol) calculated by LDA [18], reflecting the effect of strong mass renormalization. The experimentally obtained  $\gamma$  coefficient in the parent compound SrFe<sub>2</sub>As<sub>2</sub> is 6.5 mJ/K<sup>2</sup>mol [15], which is expected to be significantly reduced since large portions of FS sheets are gapped [31, 32]. The normal state  $\gamma$  coefficient in the superconducting Ba<sub>0.6</sub>K<sub>0.4</sub>Fe<sub>2</sub>As<sub>2</sub>, although difficult to obtain due to its high critical field ( $H_{c2}$ ), was estimated to be as large as  $\sim 63$  mJ/K<sup>2</sup>mol [34].

In conclusion, we have fully determined the band structure and Fermi surfaces of the optimally doped Fe-based superconductor Ba<sub>0.6</sub>K<sub>0.4</sub>Fe<sub>2</sub>As<sub>2</sub>. Four dispersive bands in the vicinity of  $E_F$  have been clearly observed, resulting in two hole-like FSs (with a possible third degenerated FS) around  $\Gamma$  and two electron-like FSs around M. The two electron-like FSs are consistent with the unexpected hybridization of the two overlapping orthogonal elliptic FSs, resulting in the outer ( $\delta$ ) FS being nearly nested with the inner hole-like ( $\alpha$ ) FS via the  $(\pi, \pi)$  AF wavevector. In contrast to the LDA, only small  $k_z$  dispersions are observed for the FSs, with the total volume consistent with Luttinger theorem. Furthermore, the overall bandwidth is renormalized by a factor of 2, while the low energy dispersions acquire an

even stronger renormalization effect that implies a much enhanced specific heat coefficient  $\gamma \sim 32$  mJ/K<sup>2</sup>mol calculated using the tight-binding band parameters obtained from fitting the observed electronic structure. The comparison of our measured band dispersions with those predicted by LDA provides valuable insights into the possible effects of electronic correlations, a central unresolved issue in the field of iron pnictides.

This work was supported by grants from Chinese Academy of Sciences, NSF, Ministry of Science and Technology of China, JSPS, TRIP-JST, CREST-JST, MEXT of Japan, and NSF (DMR-0800641, DMR-0704545), DOE (DEFG02-99ER45747) of the US. This work is based upon research conducted at the Synchrotron Radiation Center supported by NSF DMR-0537588, and the Advanced Light Source supported by DOE No. DE-AC02-05CH11231.

- 
- [1] Y. Kamihara *et al.*, *J. Am. Chem. Soc.* **130**, 3296 (2008).
  - [2] C. de la Cruz *et al.*, *Nature* **453**, 899 (2008).
  - [3] D.J. Singh and M.H. Du, *Phys. Rev. Lett.* **100**, 237003 (2008).
  - [4] F. Ma and Z.-Y. Lu, *Phys. Rev. B* **78**, 033111 (2008).
  - [5] G. Xu *et al.*, arXiv:0807.1401.
  - [6] I.I. Mazin *et al.*, arXiv:0806.1869.
  - [7] H. Ding *et al.*, *Eur. Phys. Lett.* **83** 47001 (2008).
  - [8] C. Liu *et al.*, arXiv:0806.2147.
  - [9] L.X. Yang *et al.*, arXiv:0806.2627.
  - [10] C. Liu *et al.*, arXiv:0806.3453.
  - [11] L. Zhao *et al.*, arXiv:0807.0398.
  - [12] D.H. Lu *et al.*, *Nature*, **455**, 81 (2008).
  - [13] V.B. Zabolotnyy *et al.*, arXiv:0808.2898.
  - [14] L. Wray *et al.*, arXiv:0808.2185.
  - [15] G.F. Chen *et al.*, arXiv:0806.2648.
  - [16] D.E. Eastman *et al.*, *Phys. Rev. Lett.* **45**, 656 (1980).
  - [17] R.J. Lad and V.E. Henrich, *Phys. Rev. B* **39**, 13478 (1989).
  - [18] F. Ma, Z.-Y. Lu, and T. Xiang, arXiv:0806.3526.
  - [19] We caution that some ordinate Auger intensity will be also included in the difference curve.



- [20] K. Haule, J.H. Shim, and G. Kotliar, *Phys. Rev. Lett.* **100**, 226402 (2008).
- [21] H.-B. Yang *et al.*, *Phys. Rev. Lett.* **95**, 146401 (2005).
- [22] H.Q. Yuan *et al.*, arXiv:0807.3137.
- [23] S. Weyeneth *et al.*, arXiv:0811.4047.
- [24] T. Valla *et al.*, *Science* **285**,2110 (1999).
- [25] U. Welp *et al.*, arXiv:0810.1944.
- [26] M.M. Korshunov and I. Eremin, *Phys. Rev. B* **78**, 140509(R) (2008).
- [27] I.I. Mazin *et al.*, *Phys. Rev. Lett.* **101**, 057003 (2008).
- [28] K. Kuroki *et al.*, *Phys. Rev. Lett.* **101**, 087004 (2008).
- [29] F. Wang *et al.*, arXiv:0807.0498.
- [30] K. Seo, B.A. Bernevig, and J.P. Hu, *Phys. Rev. Lett.* **101**, 206404 (2008).
- [31] J. Dong *et al.*, *Eur. Phys. Lett.* **83**, 27006 (2008).
- [32] S.E. Sebastian *et al.*, *J. Phys.: Cond. Mat* **20** 422203 (2008).
- [33] K. Nakayama *et al.*, in preparation.
- [34] G. Mu *et al.*, arXiv:0808.2941.

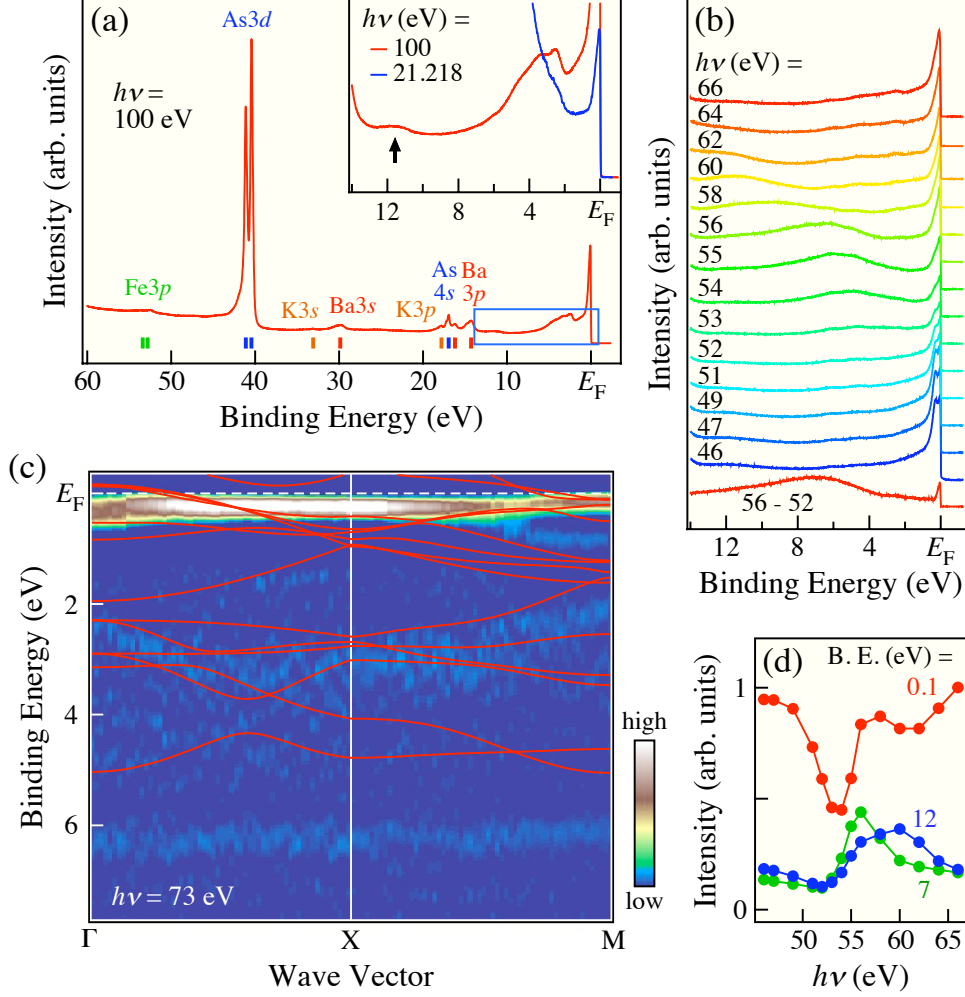


FIG. 1: Shallow core levels and valence band of  $\text{Ba}_{0.6}\text{K}_{0.4}\text{Fe}_2\text{As}_2$ . (a) Wide range EDC near  $\Gamma$  ( $h\nu = 100$  eV) showing many shallow core levels, whose atomic energy levels are marked by vertical bars above the  $x$ -axis. The inset magnifies the valence band and a possible satellite peak at  $\sim 12$  eV, and highlights the difference between spectra taken at 100 and 21.2 eV. (b) Valence band near  $\Gamma$  measured at different photon energies (46 - 66 eV). The red spectrum at the bottom is the difference between EDCs measured at 56 (at resonance) and 52 eV (below resonance). All EDCs are normalized by the photon flux. (c) Intensity plot of second derivatives of spectra along  $\Gamma$ -X and X-M ( $h\nu = 73$  eV). LDA bands (red lines) are also plotted for comparison. (d) Photon energy dependence of the intensity of EDCs shown in Fig. 1b, obtained at the binding energies of 0.1, 7, and 12 eV .

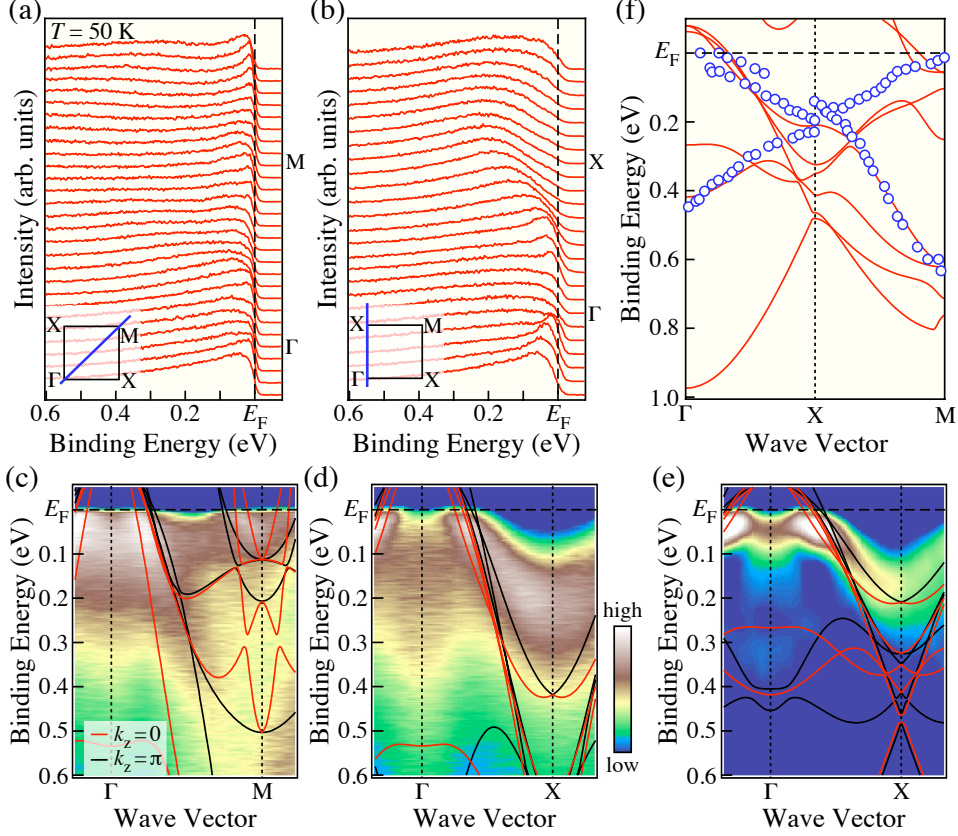


FIG. 2: Coherent Fe  $3d$  spectra within 0.6 eV from  $E_F$  measured at 50 K along  $\Gamma$ -M and  $\Gamma$ -X. EDCs along (a)  $\Gamma$ -M and (b)  $\Gamma$ -X ( $h\nu = 21.2$  eV). Intensity plots of the same spectra along (c)  $\Gamma$ -M and (d)  $\Gamma$ -X. LDA calculated bands at  $k_z = 0$  (red) and  $k_z = \pi$  (black) are also plotted for comparison. (e) Intensity plot of second derivatives of the spectra along  $\Gamma$ -X in comparison with the LDA bands renormalized by a factor of 2. (f) Extracted band positions (blue circles) measured at 45 eV along  $\Gamma$ -X-M with the comparison to the same renormalized LDA bands of  $k_z = 0$ .

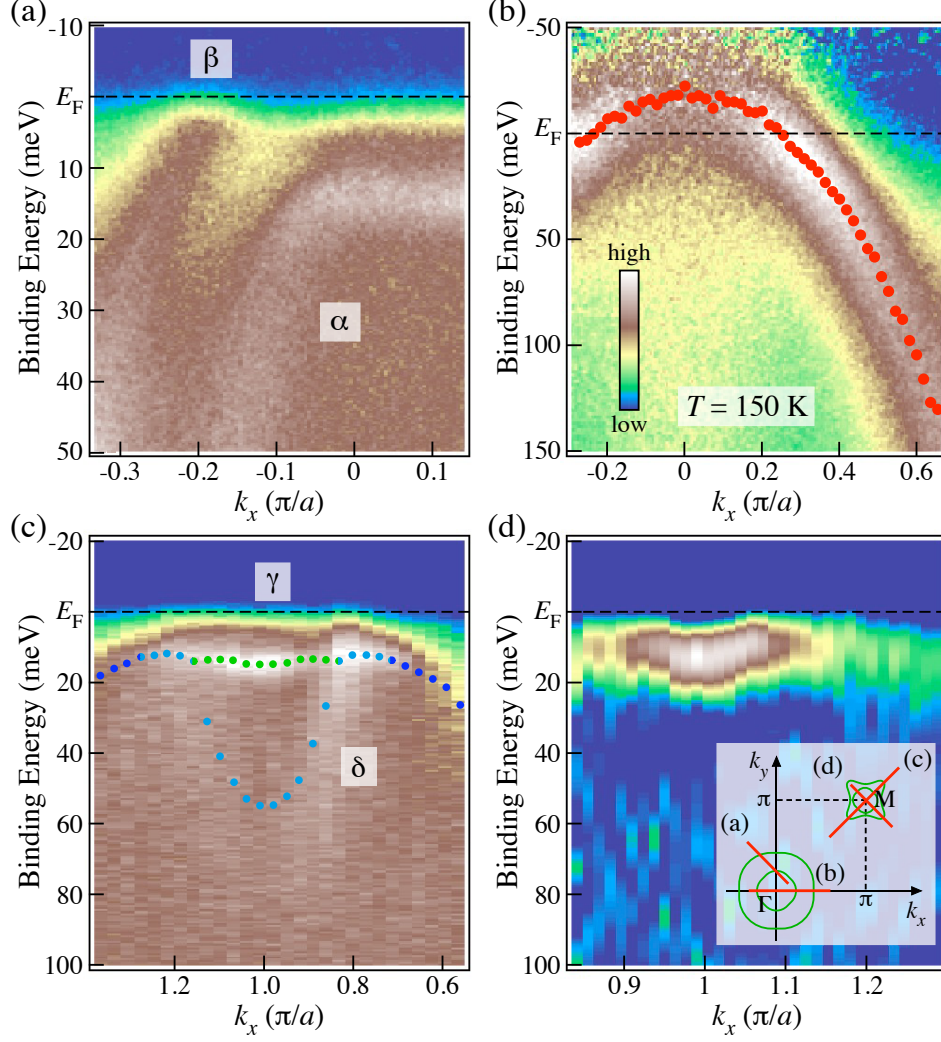


FIG. 3: Low-energy fine structures of  $\text{Ba}_{0.6}\text{K}_{0.4}\text{Fe}_2\text{As}_2$ . (a) Intensity plot near  $\Gamma$  measured at low temperature ( $T = 15$  K) clearly displaying two hole-like ( $\alpha$  and  $\beta$ ) bands approaching  $E_F$ . (b) Intensity plot near  $\Gamma$  measured at high temperature ( $T = 150$  K) divided by the Fermi function, showing that the band top of the  $\alpha$  band is  $\sim 20$  meV above  $E_F$ . The red dots are band positions extracted from EDC peaks. (c) Intensity plot in the vicinity of M measured at 15 K showing two electron-like ( $\gamma$  and  $\delta$ ) bands and a hole-like band dispersion approaching  $E_F$  (see blue dots). The dots are EDC peak positions. (d) Intensity plot of second derivatives of the spectra near M, indicating the electron-like nature of the  $\gamma$  band. The inset indicates measurement locations in the BZ for panels (a) - (d).

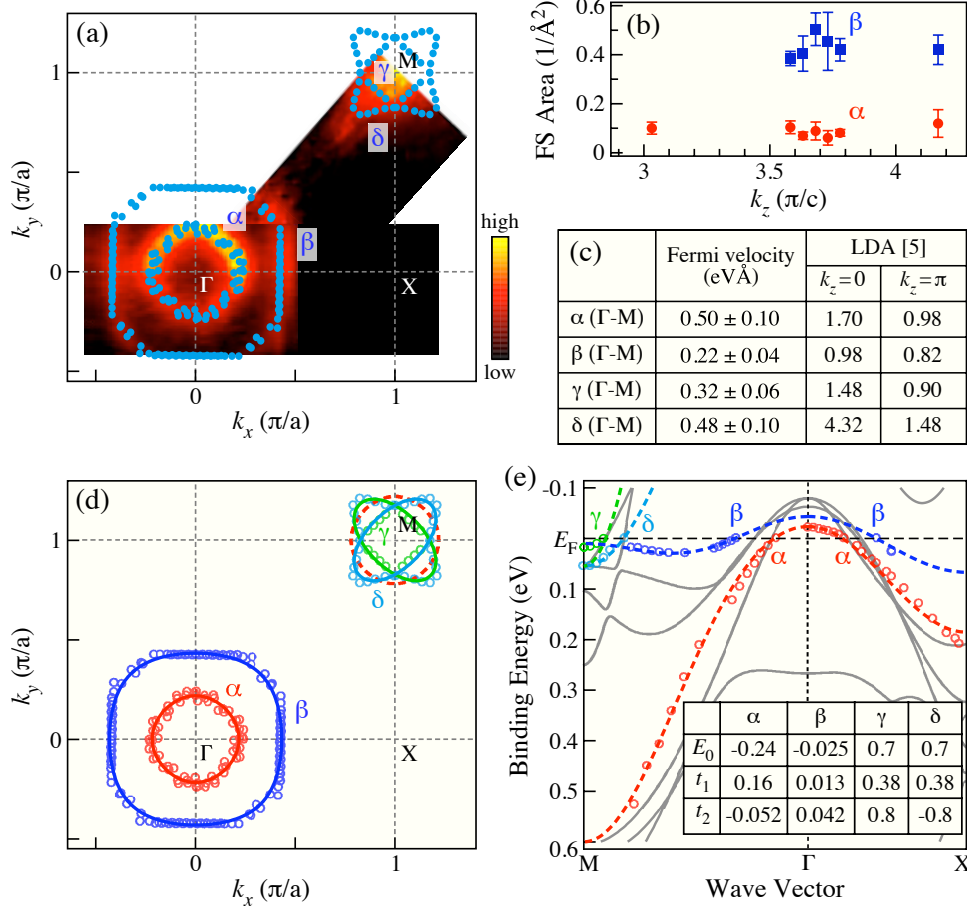


FIG. 4: Summary of measured FSs and band structure. (a) FSs on the 2D BZ obtained from the intensity integrated within  $E_F \pm 10$  meV (false color plot) and the Fermi crossing points (blue dots) obtained from MDC and EDC dispersions. (b)  $k_z$  dispersion of the  $\alpha$  and  $\beta$  FS areas obtained by changing photon energy. (c) Table of the measured and calculated Fermi velocities along principle axes. (d) Measured FS (circles) and tight-binding fitting curves (solid lines). The dashed line is the fitted  $\alpha$  FS shifted by the  $(\pi, \pi)$  wavevector. (e) Measured band dispersion (circles) along  $\Gamma$ -M and  $\Gamma$ -X, compared with the LDA bands renormalized by a factor of 2 (solid lines), and tight-binding fits (dashed lines). The inserted table lists the parameters of tight-binding bands.